K-shell X-ray Spectroscopy of Laser produced Aluminum Plasma

Channprit Kaur[1], S.Chaurasia[1*], A.K. Poswal[2], D.S. Munda[1], A.K. Rossall[3], M.N.Deo[1], S. M. Sharma[1]

[1]*High Pressure & Synchrotron Radiation Physics Division, Bhabha Atomic Research Centre, Mumbai – 400085, India*
[2]*Atomic & Molecular Physics Division, Bhabha Atomic Research Centre, Mumbai – 400085, India*
[3]*International Institute for Accelerator Applications, The University of Huddersfield, Queensgate, Huddersfield, HD1 3DH, UK*

(Email:pgshivanand@gmail.com)

Abstract

Optimization of a laser produced plasma (LPP) X-ray source has been performed by analyzing K-shell emission spectra of Al plasma at a laser intensity of 10^{13}-10^{14} W/cm^2. The effect of varying the laser intensity on the emissivity of the K-shell resonance lines is studied and found to follow a power law, $E \alpha I^{\alpha}$ with α=2.2, 2.3, 2.4 for He_{β}, He_{γ}, He_{δ} respectively. The emission of these resonance lines has been found to be heavily anisotropic. A Python language based code has been developed to generate an intensity profile of K-shell spectral lines from the raw data. In theoretical calculations, the temperature is estimated by taking the ratio of the Li-like satellite ($1s^2$2p-1s2p3p) and the He_{β} ($1s^2$-1s3p) resonance line and the ratio of the He-like satellite (1s2p-$2p^2$) and the Ly_{α} (1s-2p) resonance line. To determine the plasma density, stark broadening of the Ly_{β} spectral line is used. Simulation was carried out using the FLYCHK code to generate a synthetic emission spectrum. The results obtained by FLYCHK are T_e=160 eV, T_h=1 keV, f=0.008, n_e=5 x 10^{20} cm^{-3} and the analytical model resulted T_e=260-419 eV and n_e=3x10^{20} cm^{-3}.

Key words: Laser produced plasma, K-shell X-ray spectrum, Plasma parameters, Angular distribution

1. Introduction

Laser produced plasma (LPP) is a brilliant source for X-ray production. The high density and temperature of plasma produced by focusing a high power laser makes it an ideal media for production of X-ray sources. These X-rays have several applications in various fields of science. These X-ray sources can be used as a probe for the study of high density phenomenon by using them as a back-lighter in extreme matter physics [1] which allows us to determine the opacity of materials [2]. Opacity plays a key role in radiation diffusion modeling of stars [3] and in inertial confinement fusion (ICF) for accurate modeling of radiative hydrodynamics. The use of these LPP X-rays in X-ray radiography of shocked material which is opaque to optical light [4-5], lithography [6], X-ray microscopy [7], radiobiology [8], photo pumped X-ray lasing, efficient soft X-ray emission for indirect drive fusion scheme [9] etc. shows its importance. Optimization of these X-ray sources is essential for the development of effective and compact X-ray sources. The X-ray line spectra emitted from hot dense plasmas provide an important diagnostic tool to infer local plasma parameters such as temperature, density and ionization states. Many authors have successfully theoretically and experimentally analyzed the spectra [10-11] emitted from dense plasmas of various materials irradiated with intense laser pulses. K-shell spectra, including resonance lines of Hydrogen (1s-np, $n > 2$) and Helium ($1s^2$-1snp, $n > 2$) like ions (H-like and He-like) along with associated satellites are particularly interesting because the spectrum is relatively simple and easy to model. High precision numerical calculations of various atomic characteristics make these spectra a convenient tool for the investigation of physical processes occurring in the solar corona [12].These resonance lines, also known as ionic lines, are due to the transition of electrons in highly charged species present in plasma such as H-like, He-like etc. There has been considerable interest in satellite emission appearing on the long wavelength side of resonance lines. These satellites, arising from doubly excited configurations, are particularly useful as a diagnostic tool because they are less sensitive to opacity effects. The relative intensity of these satellites to their parent resonance line provides a valuable diagnostic for the measurement of various plasma parameters. These dielectronic satellites of spectral lines of multiply

charged ions have been investigated actively during the last several years [13-15]. There are also several calculations have been done using a multi-configuration Dirac–Fock method with the addition of quantum electrodynamics as well as Breit corrections to estimate density and temperature of plasmas using Li-like ions of mid Z [16-17]. In general, the X-ray emission from a planar target irradiated with an intense laser is considered as isotropic and several models use this basis. It has been shown that there is a large deviation from the isotropic nature of Bremsstrahlung X-ray flux due to a change in plasma opacity with respect to target normal [18].

In this paper, a detailed study of the K-shell X-ray emission spectrum generated by 30 J, 500 ps Nd: Glass laser, focused to an intensity of 10^{13}-$2x10^{14}$ W/cm^2 is presented. The angular dependency of K-shell resonance lines flux of the Al plasma has been studied by rotating the target normal with respect to detector.

2. **Experimental setup:**

The experiment was carried out using Nd: Glass laser which provides an output energy of 30 J per pulse with pulse duration of 500 ps. The laser was incident on a 10 mm thick Al slab and focused to a spot size of 120 μm using an f/5 lens, yielding a peak intensity of $2x10^{14}$ W/cm^2. The experimental chamber was evacuated to a pressure $4x10^{-5}$ mbar. An X-ray crystal spectrometer using a Thallium Acid Phthalate (TAP) crystal placed at 45^o with respect to laser axis was used for the line emission studies in spectral range of 5.5-7.5Å which enabled us to measure He-β, γ, δ, ε and H-like lines. These resonance lines are due to Al XII, Al XIII and Al XIV ions. Two stacked aluminized polycarbonate foils (Alexander Vacuum Research, Inc., trade name: B-10) having 1/e cutoff of 0.9 keV were used to prevent the scattered visible light from entering the plasma chamber. The TAP crystal spectrally resolves X-ray emission from the laser produced plasma, these reflected X-rays were detected by X-ray CCD camera (Model VISION 4M, from Rigaku innovative) having resolution of 25 mÅ. To obtain a wide range of X-ray energies, the spectrum crystal is mounted on a motorized Z-stage which can move up and down by 15 mm. By

changing the height of the crystal with respect to the plasma we are able to cover a spectral range of 5.5-7.5Å. A schematic of the crystal spectrometer along with the experimental setup is shown in Figure 1a. A sample image of one recorded X-ray spectrum is shown in Figure 1b. The X-ray spectra were analyzed using a code developed by our group using Python software. To facilitate the angular distribution studies, the target was mounted on the motorized X-Y-Z-θ stages. The angular distribution of K-shell resonance lines with associated its satellites and Al XII, Al XIII and Al XIV ions are studied by mounting the X-ray crystal spectrometer and Thomson parabola spectrometer (TPS) at 45^0 on each of the laser axis when target normal and laser axis are collinear.

Two ion collectors are installed at an angle of 22.5^0 and 45^0 with respect to target normal to measure the ion temperature and plasma expansion velocity. The schematic of ion collector is shown in Figure 1c. Our ion collector is the simplest and most common type of probe with a plane collector and a grid for ion and electron separation. The separation is done by means of a static field that exists between the grounded grid and the biased (negative) collector, which will solve the problem of the contribution of secondary electron emission and as the Faraday cup has a large area, it can be placed far away from the target to give better resolution. The grid also separates primary electrons from the ions to be measured. The ion collector signal can be written as

$$I_{coll}(t) = \frac{U_c(t)}{\left\{\varepsilon R_{load}\left[1+\frac{\bar{\gamma}(t)}{\bar{z}(t)}\right]\right\}} = \frac{ed[N(t)\bar{z}(t)]}{\bar{z}(t)} \qquad (1)$$

where $U_c(t)$ is the voltage amplitude of the collector signal on oscilloscope, N(t) is the number of ions reaching the charge collector and R_{load} is the load resistance, ε is transparency of entrance grid. The time distribution of ion charge Q can be written as

$$\frac{dQ}{dt} = \frac{ed[N(t)\bar{z}(t)]}{dt} \rightarrow I_{coll}(t) = \frac{U_c(t)}{\left\{\varepsilon R_{load}\left[1+\frac{\bar{\gamma}(t)}{\bar{z}(t)}\right]\right\}} \qquad (2)$$

The factor $\left[1+\frac{\bar{\gamma}(t)}{\bar{z}(t)}\right]$ = 1.5 for v =7 x 10^6 cm/sec),

= 1.0 for v>1 x 10^7 cm/sec,

and = 0.5 for intermediate velocity,

The ion velocity and energy were obtained by measuring the time of flight (TOF) spectrum of ions as shown in Figure 1d.We have verified our measurement by comparing with the results from a TPS which provide energy spectrum of individual charge states of Al.

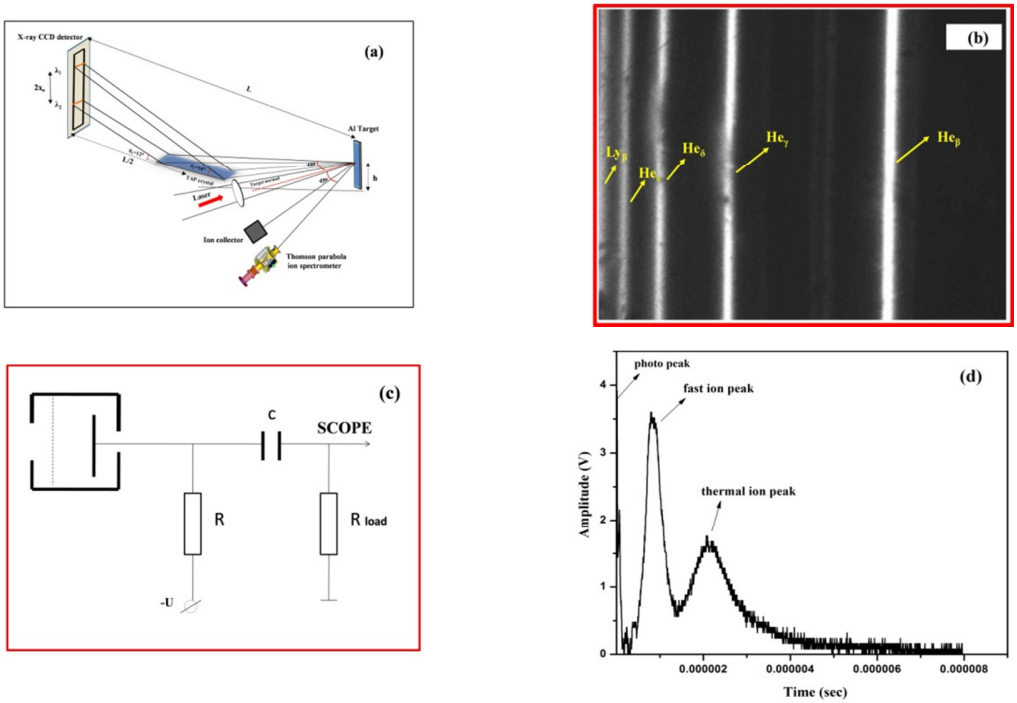

Figure 1(a) Schematic of experimental set up along with crystal spectrometer and ion collector **(b)** Image of X-ray spectrum recorded by X-ray CCD camera, **(c)** Schematic of flat plate type Faraday cup **(d)** Ion collector signal recorded on oscilloscope.

2.1 Crystal spectrometer:

Crystal spectrograph with flat crystals are widely used to measure the X-ray spectrum emitted from laser produced plasmas due to a straight forward alignment process and the relative ease of operation. The basic principle of an X-ray crystal spectrometer is the Bragg reflection from the crystal planes given by formula $2dsin\theta = n\lambda$, where d is the separation between parallel reflecting planes of the crystal, n is the order of reflection (n=1,2,3…), and θ is the Bragg angle.

When the X-ray source is a point source and collimated, the X-ray spectrum can be recorded by rotating the crystal. However, in a laser produced plasma, it is a spherically expanding plasma which subtends a range of angles at different positions on the crystals. The wavelengths satisfying Bragg's condition result in a spectrally dispersed spectrum on detector plane (X-ray CCD). If θ_1 and θ_2 are angles subtended by X-rays at either ends of crystal then according to Bragg's law we will get minimum and maximum wavelengths given by

$$\lambda_1 = 2dsin\theta_1 \quad (3)$$

$$\lambda_2 = 2dsin\theta_2 \quad (4)$$

These wavelengths can be written as follow in terms of geometric parameters

$$\lambda_1 = 2d(2h + x_0)/[(2h + x_0)^2 + L^2]^{1/2} \quad (5)$$

$$\lambda_2 = 2d(2h - x_0)/[(2h - x_0)^2 + L^2]^{1/2} \quad (6)$$

Where $2x_0$ is the detector size, h is vertical height of plasma source with respect to crystal, L/2 is the horizontal distance between plasma source and centre of crystal (L is the distance between source and detector) as shown in Figure 1a. The spectral resolution of crystal spectrometer can be written as

$$\Delta\lambda = \frac{2d}{[1+(2h/L)^2]^{1/2}}[\delta\theta + \delta x/L[1 + (^{2h}/_{L})^2] \quad (7)$$

where $\Delta\lambda$ is the wavelength interval covered by ideally monochromatic X-rays from a source detected after Bragg reflection from a crystal. The first term in the square bracket is the crystal dependent term (rocking curve) which is 0.45 mrad for TAP crystal at 8Å and second term depends on source and detector's characteristics.

The spectrum resolution of a crystal depends on the source size, distance between source and detector and the rocking angle of the crystal. Therefore, it is clear that for a fixed focal spot diameter (i.e. a fixed source size) if we increase distance between source and detector, the resolution of the spectrometer will increase linearly with distance however, at the same time X-ray flux reduces according

to $1/L^2$. Optimization is necessary between the X-ray flux and distance between source and detector. The spectral range covered for a particular position of crystal will be reduced. In our experiment, we modified our experimental chamber and adjusted the distance between the source and detector to obtain a higher resolution for the study of a strong X-ray flux from the K-shell of an Al plasma. For flexibility in the spectral range covered, we have mounted our target on motorized Z-stage. Spectral range can be changed from 5.5 Å to 7.5Å by changing the vertical distance between plasma source and crystal, though spectral range covered for a single setting is less than 1Å as shown in Figure 2a-d. In the present experiment, a TAP (thallium acid phthalate) crystal with (001) plane of size 50 x 10 mm^2 with a thickness of 2 mm is used and had a 2d spacing of 25.75 Å. The crystal was kept at a distance of 175 cm from the target. The source to detector distance is 350 cm. The detector unit was mounted on a flange having a taper angle of 15^o and was connected to the port of the vacuum chamber. The recording system i.e. X-ray CCD camera with KF 50 flange was mounted on the chamber.

3. Results and discussion

3.1. Code for image processing:

In our experiment, we have used a soft X-ray scientific digital CCD camera from Rigaku (Model X-VISION – 4M) Czech Republic for the detection of X-ray lines. The CCD image sensor is a back illuminated sensor with 2048 x 2048 pixels. The pixel size is 13.5 μm x13.5 μm and the image area dimension is 27.6 mm x 27.6 mm. The CCD uses a 16 bit readout unit with readout speed of 25 Kpixels/sec so it takes ~168 second to read all pixels. The readings are initially stored in detector's onboard memory and after finishing readout; data is transferred to the PC using parallel port.

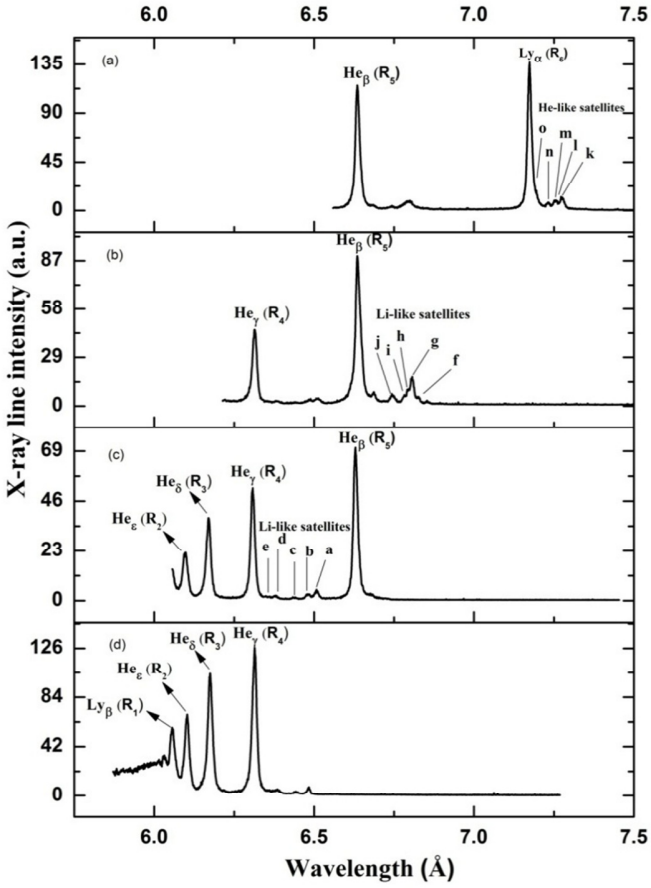

Figure 2.(a-d) K-shell X-ray line emission spectrum form Al plasma showing different range of wavelength covered by changing the distance between plasma source and the TAP crystal.

The camera is provided with proprietary software, which collects data and saves it as a raw image without compression loss or a BMP image of 8 bit resolution with some compression. Whilst analyzing data with the images provided by this software, we faced two serious difficulties. Firstly, the software can export the image in BMP format with 8-bit integer values but not in ASCII format, so we lose information. Since the BMP images have lower resolution, it is always preferable to use the raw file to analyze data. Secondly, the proprietary software has the option of full binning but it imposes a serious drawback of readout saturation due to a large collection of charge from a whole column of pixels and limited range of readout unit. Additionally, the illumination of CCD is in a 2/3rd region so while binning

an un-illuminated region can contribute to a false signal. To overcome these shortcomings, we have developed software using the Python language to handle the raw data files. Firstly, this code imports the raw data file with full 16 bit resolution without any compression loss. Two dimensional image data is recorded and each column of pixels corresponds to same energy, so several pixels with same energy are added to reduce the noise in recorded spectra. In this manner, the noise is reduced by factor of $\sqrt{n}$, where n is the number of rows (In our case n=100) added to get spectrum. Figure 3 shows the comparative spectrum processed by freely available image processing software PROMISE [19] and our code. From the figure it is clear that data processed by other software is showing saturation whereas with our code we are getting an unsaturated spectrum which is beneficial to calculate the X-ray line flux quantitatively.

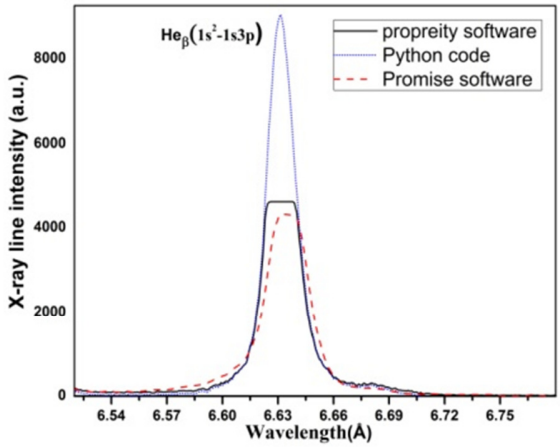

Figure 3: Processed intensity plot of He_β line with 8 bit BMP(—), Promise (-----) and Python (…) software developed by our group.

3.2. Scaling with respect to energy:

The study of X-ray conversion efficiency as a function of different parameters such as laser energy and the variation in focal spot size plays a key role in the optimization of a LPP X-ray source. Laser intensity can be varied by two methods; one is changing the laser energy whilst keeping laser spot size and the laser pulse duration fixed and the other method is by defocusing the laser on target whilst keeping a constant laser energy and pulse duration [20]. In the latter case, laser intensity increases as we move

towards best focus position due to a reduction in beam diameter. In [21], it is shown that changing the laser energy is a more efficient method to increase the conversion of laser energy into X-rays. In our case, we have studied the K-shell X-ray line emission yield from Al plasma as a function of laser intensity keeping the laser pulse duration and laser focal spot size fixed at 500 ps and 120 μm respectively. The He_β, He_γ, He_δ intensities as a function of laser intensity is shown in Figure 4. It scales as $I_x = (I_L)^\alpha$,where, I_x is the X-ray flux of different K-shell resonance lines of He-like Al, I_L is intensity of laser and α is a scaling exponent. The scaling component α has been calculated for all resonance lines and found to be 2.2, 2.2, 2.3 for He_β, He_γ, He_δ respectively, which is in the same range as reported in earlier publication [22]. The increase in resonance line yield can be inferred from the fact that as the laser intensity increases, the temperature and thus thermal emission rapidly increases resulting in an enhancement in ionic line intensities. Due to a relatively long pulse, 500 ps in our case, the interaction time of the laser with the plasma is long, which gives rise to a higher scaling of lines as compared to ultra-short pulses in which laser interacts with plasma for very small time [23].

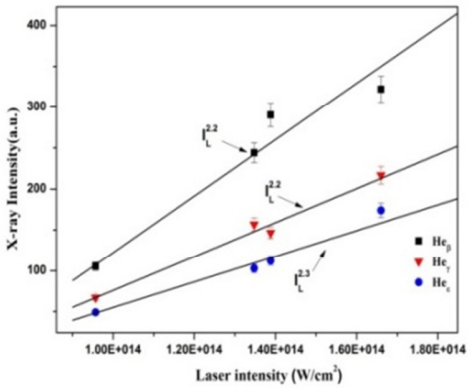

Figure 4.Figure showing variation of intensity of He_β, He_γ, He_δ spectral lines as function of laser intensity

3.3. Measurement of plasma parameters:

The intensity of various resonance lines (Ly_{α}, Ly_{β}, He_{β}, $He_{\gamma,}$ etc.) and associated satellites and the plasma parameters calculated using various models and simulations are discussed below.

3.3.1. Temperature estimation:

The ratio of a satellite line to its parent resonance line is a good diagnostic for the estimation of plasma temperatures. Satellites are formed from doubly excited levels in He-like and Li-like ions. Transitions from these doubly excited levels appear on the long wavelength side of the resonance lines of H-like and He-like ions. These are resonance transitions in the presence of an additional electron in the excited state known as spectator electron. There will be a number of satellites depending upon the excited state of this spectator electron, but the most intense and distinguishable satellite will arise from transitions having a spectator electron in the n=2 excited state. For higher values of n, these satellites become inseparable from its parent resonance line. In the case of H-like ions, the main transition i.e.1s-np will take place in the presence of a spectator electron in the n'l' state i.e. nln'l'-1sn'l' (transition from He-like ions). In case of He-like ions, there are two channels of radiative decay of doubly excited states from the $1s2l3l'$ state, one is the $1s^2 2l$ (satellite to He_{β} resonance line) and the other is $1s^2 3l$ (satellite to He_{α} resonance line). In the past, plasma parameters have been largely estimated using the He_{α} line and its satellite. We have estimated the plasma temperature using the He_{β} and Ly_{α} lines and their corresponding satellites using the model described in [22], which is more appropriate as the opacity effect is less for transitions with higher n values.

The intensities of Li-like satellites are proportional to rate coefficients for dielectronic recombination and the fractional abundance of He-like ions. The ratio of intensities of a Li-like satellite to a He-like resonance line is independent of the fractional abundance of the He-like ions but strongly depends upon temperature as resonance lines are produced by electron impact excitation. The intensity of the satellite line is given by [25-26]

$$I_{sat} = N_{He} N_e C_{diel} \frac{A_{rad}}{A_{auto}+A_{rad}} \quad (8)$$

where N_{He} and N_e are the densities of the He-like ion ground state and electrons respectively. C_{diel} is the dielectronic capture rate coefficient. The value $\frac{A_{rad}}{A_{auto}+A_{rad}}$ is the branching ratio for the decay of a satellite level by radiation (A_{rad}) against the auto-ionization rate (A_{auto}). The ratio of dielectronic capture rate to autoionization rate is given by the principle of detailed balance

$$\frac{C_{diel}}{A_{auto}} = \frac{h^3}{2(2\pi mkT)^{3/2}} \frac{g_s}{g_1} \exp(-E_{sat}/kT) \quad (9)$$

where g_s , g_1 are the statistical weights of the satellite level and the He-like ion ground state respectively, E_{sat} is the energy difference between these, T is electron temperature, *h*, *m* and *k* are Plank's constant, mass of electron and Boltzmann constant respectively. Therefore, the satellite intensity is given by,

$$I_{sat} = N_{He} N_e \frac{4\pi^{3/2} {a_0}^3}{T^{3/2}} \frac{g_s}{g_1} \frac{A_{rad} A_{auto}}{A_{auto}+A_{rad}} \exp(-E_{sat}/kT). \quad (10)$$

The intensity of the He-like ion resonance line is given as

$$I_{res} = N_{He} N_e (C_{coll} + D_{diel}) \quad (11)$$

where C_{coll} is the collisional excitation rate coefficient and D_{diel} is the additional contribution of dielectronic recombination. After substituting all parameters, the intensity of the resonance line is given as

$$I_{res} = \frac{\sqrt{3}}{2} \pi \frac{m {a_0}^2}{h} A_r \frac{E_0}{TfP} \frac{g_s}{g_1} \exp(-E_{res}/kT) \frac{1}{1+\alpha} \quad (12)$$

where α ~D/C, *f* is the oscillator strength for excitation of resonance line, P is the gaunt factor.

Therefore, the relative intensity of a satellite to its resonance line is given as

$$\frac{I_{Sat}}{I_{res}} = \frac{\sqrt{3} m \pi {a_0}^2}{h} \frac{1}{fP} \frac{E_{res}}{kT} \frac{g_s}{g_1} \frac{A_r A_a}{A_a+\Sigma A_r} \exp\left[\frac{E_{res}-E_{sat}}{kT}\right] (1+\alpha). \quad (13)$$

Here α is a correction factor which gives the contribution of unresolved satellites, after omitting the term (1+α) and taking $f \sim 0.55$ and $P \sim 0.2$ with T in eV, equation (13) can be expressed as

$$\frac{I_{Sat}}{I_{res}} = 953.7 \times 10^{-19} \frac{E_{res}}{T} \frac{g_{sat}}{g_1} \frac{A_{rad}A_{auto}}{A_{auto}+\Sigma A_{rad}} \exp\left[\frac{E_{res}-E_{sat}}{kT}\right] \quad (14)$$

where E_{res} and E_{sat} are energies of the resonance line and the satellite line above the ground state of a He-like ion. The ratio of the intensities of satellite lines and their resonance line were compared with data provided in reference [24]. Calculated temperatures for various satellites and resonance lines are given in the last column of the Table 1. From Table 1, it can be seen that the plasma temperature estimated by H-like ions is more than the temperature estimated from the He-like ions. The reason for this is the spatial position of the occurrence of the formation of H-like and He-like ions. H-like ions are formed near the critical density where maximum laser energy is deposited. However, He-like ions are from the extended portion of the plasmas where the plasma temperature is lower. The temperature estimated by H-like ions is more reliable than He-like ions because the doubly excited level of Li-like ions can be populated in two ways (i) by dielectronic recombination and (ii) by the direct excitation from the inner shell of a Li-like ion. In this case the equation (14) may underestimate the electron temperature.

Table1. Transitions and Wavelengths of H like and He like spectral lines with satellites along with their branching ratio and calculated plasma temperature using equation (14).

Key	**Wavelength λ(Å)**	**Transition**	**Branching Ratio** $g_s \frac{A_{rad}A_{auto}}{A_{auto}+\Sigma A_{rad}}$**(x10^{13})**	**I_{sat}/I_{res}**	**Temperature(eV)**
R_1(Ly_β)	6.05	1s-3p			
R_2 (He_ε)	6.10	$1s^2$-1s6p			
R_3(He_δ)	6.17	$1s^2$-1s5p			
R_4(He_γ)	6.31	$1s^{21}$S-1s4p ^{1}P			
a	6.51	$1s^2$2p ^{2}P-1s2p4p ^{2}D			
b,c,d,e	6.48,6.44, 6.38, 6.36	$1s^2$3l-1s4p3l			
R_5(He_β)	6.63	$1s^2$ $^1S_0$-1s3p $^1P_1$		1	

f	6.83	$1s^22p\ ^2P$ -$1s2p(^3P)3p\ ^2P$	0.016	0.059	267
g	6.81	$1s^22p\ ^2P$ -$1s2p(^3P)3p\ ^2D$	0.09	0.19	279
h	6.74	$1s^22p\ ^2P$ -$1s2p(^3P)3p\ ^2S_{1/2}$	0.25	0.11	370
i		$1s^22p\ ^2P$ -$1s2p(^3P)3p\ ^2D$			
$R_6(Ly_\alpha)$	7.17	$1s\ ^2S_{1/2}$-$2p\ ^2P_{3/2}$			
k	7.27	$1s2p\ ^1P_1$-$2p^2\ ^1D_2$	15.22	0.091	419
l	7.26	$1s2p\ ^3P$-$2p^{23}P$			
m	7.25	$1s2s\ ^3S_1$-$2s2p\ ^3P$			
n	7.23	$1s2s\ ^1S_0$-$2s2p\ ^1P_1$			
		$1s2p\ ^1P_1$-$2p^{21}S_0$			
o	7.19	$1s3p\ ^{1,3}P$-$2p3p\ ^{1,3}P\ ^{1,3}D$			
		$1s3s\ ^{1,3}S$-$2p3s\ ^{1,3}P$			

3.3.2. Density estimation:

The broadening of ionic lines, especially Lyman and Balmer lines (which originate from Al XIII from 1s-np state) are appropriate for the determination of density. Many factors contribute to the broadening of ionic lines such as quasi-static broadening by ions, contribution of electron impact, Doppler effect and Debye screening. Contribution of electron impact is negligible in a laser produced plasma. The main broadening factors are Doppler broadening and ion impact i.e. the Debye screening. We have used the Ly_β resonance line (1s – 3p), where n = 3. The effect of opacity on this line intensity is less than Ly_α due to higher n value transitions, which has a lower oscillator strength. Another reason for choosing the Ly_β line is that the determination of density from Stark broadening is only possible with a shorter distance from the target. Resonance lines of H- like ions are emitting from the area closer to the target. For greater distances, the error in the subtraction of the Doppler broadening resulted in a considerable error in the determination of the electron density. The Ly_β line is Lorentzian in shape [27] and in high density plasma ($> 10^{19}$ /cm^3), stark broadening is the dominant mechanism however there will be broadening due to the Doppler effect. Doppler broadening is due to the thermal motion of ions which results in a shift of emission lines up or down, depending on whether the ion is moving toward or away from the observer.

The magnitude of the shift is proportional to the velocity along the line of sight resulting in a characteristic broadening of spectral lines.

For measurement of Doppler broadening, we have used our ion collector signal and Thomson parabola spectrum for Al XII and Al XIII ions as shown in figure 1d and 6e. The thermal ion temperature from the ion collector is measured for the same laser shot which was used for X-ray measurement. The peaks given by the ion collector are of Maxwellian from which we can obtain the thermal energy and hence ion temperature. The Doppler broadening can be calculated as

$$\Delta\lambda = \frac{2\lambda}{c}\sqrt{\frac{2KT_i \ln 2}{m}} \tag{15}$$

In terms of energy scale the above formula gets converted into

$$f_G{}^{doppler} = h\Delta\nu = \frac{2h\nu}{c}\sqrt{\frac{2KT_i ln2}{m}} \tag{16}$$

where KT_i is ion temperature which is 6 keV in our case from the data of the ion collector signal, m is the atomic mass of Al, λ is wavelength of $Ly_\beta$and c is the velocity of light. Doppler broadening is found to be 2.41 eV. There is a contribution of instrumental broadening due to the dispersive element in the spectrometer, which is known as instrumental width. In our case the instrumental broadening is 3 eV, which is usually Gaussian in nature. Since instrumental and Doppler broadening is represented by Gaussian function, to calculate the cumulative effect on the spectrum, a convolution was taken using following formula [28]

$$f_G{}^{total} = \sqrt{(f_G^{inst\cdot})^2 + (f_G{}^{doppler})^2} \tag{17}$$

Using this formula, the total width of the Gaussian part is given by 3.8 eV. The profile of our Ly_β resonance line is Voigt which consists of a Gaussian profile (resulting from net effect of Doppler and instrumental broadening) and a Lorentzian profile due to stark broadening. For extracting only stark broadening we have used the following formula for the width of a Voigt profile [29]

$$f_v = 0.5346 f_{stark} + \sqrt{0.2166 f_{stark}^2 + f_G^2} \quad (18)$$

Where f_v, $f_{stark,}$ $f_G$is the FWHM of the Voigt profile, Lorentzian and Doppler respectively. By using the above formula the width of Lorentzian profile f_L i.e. Stark broadening comes out to be 3.5 eV.

Taking the Debye screening effect into consideration, the Holtzmark formula for line width is modified as [30].

$$f_{stark} \approx 0.76 (\frac{N_e}{10^{20}})^{0.6} T_e^{0.21} \quad (19)$$

where f_{stark} is Stark broadening, N_e is electron density and T_e is temperature of electrons. In this formula, for measuring electron density we need to know the temperature of the electrons. Using different values of temperature from Table 1, the density is found to be in the range of 1.6×10^{20}/cm^3 - 2.8×10^{20}/cm^3. The estimation of density from the Stark broadening is more accurate compared to using the ratio of intercombination (IC) to its resonance line (I_{IC} /I_R) [31]. The method using the ratio of I_{IC} /I_R gives a value of density close to the target that is one order of magnitude less than that calculated by Stark broadening, which is not correct. The density estimation using Stark broadening does not require the knowledge of the ionization state in contrast to the method based on I_{IC} /I_R.

We have calculated the density by using the formula [32] given below

$$f_{stark} = \left({}^{13 Z_p h}/_{2\pi Z_n m} \right) \left(n_i^2 - n_f^2 \right) (N_p)^{2/3} \quad (20)$$

where Z_p is charge of emitting ion, Z_n is the nuclear charge, N_p is density of perturbers, n_i and n_f are the quantum numbers of initial and final state respectively andm is the mass of an electron. From this, the density of ions is calculated as 2.27×10^{19}/cm^3 resulting in a density of electrons of 2.95×10^{20}/cm^3. This is in reasonable agreement with value calculated by previous method.

3.3.3. Determination of temperature and density by FLYCHK:

For the estimation of temperature and density of plasma, simulations have been done using the FLYCHK code [33] which generates a synthetic X-ray spectrum of Al. To find a best fit to the experimental spectrum, a parameter scan has been performed using a range of temperatures from 50-500eV and densities from 10^{12} to10^{21} cm^{-3}. The simulated spectra were instrument broadened with our estimated resolution (3 eV) using a post processor. The ratios of intensities of different resonance lines generated by FLYCHK at different temperatures and densities were compared with line ratios generated by the experiment. The difference between experimental ratios and theoretical ratios were plotted with respect to different temperatures as shown in Figure 5a. From the figure, it is clear that difference between the line ratios is minimum around a temperature of ~ 160eV. This code has used a two temperature (temperature of hot and cold electrons) model. Fine tuning of the synthetic spectra with experimental spectra has been done by changing the cold electron temperature to around 160 eV, the hot electron temperature scans from 0.5-1.5 keV and ratio of hot to cold electron temperature electrons from 0.005-0.1, which yields a best match of experimental and stimulated spectra at T_c=160 eV, T_h=1000 eV, f=0.008 and density $5x10^{20}$ cm^{-3}.

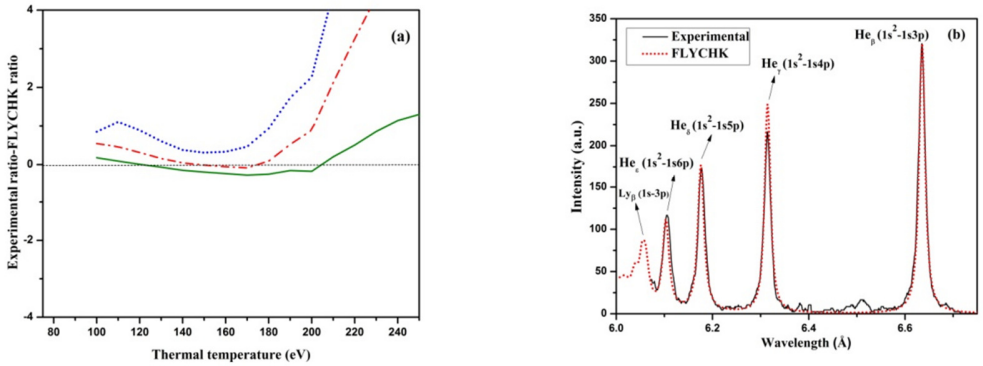

Figure 5.(a) Plot of difference between ratio of resonance lines obtained experimentally and lines generated by FLYCHK He_β/ He_γ (solid line), He_β /He_δ (dash-dotted line), He_β / He_ε (dotted line) **(b)** Experimental spectrum obtained for Aluminum plasma (solid line) and spectrum generated from

FLYCHK code (dotted lines) for T_c= 160 eV, T_h=1000 eV, f=0.008 and density $5x10^{20}$ cm^{-3}.

3.4. Conversion efficiency:

X-ray conversion efficiency indicates the amount of absorbed laser energy which is converted into X-ray flux. Laser energy absorbed by the target goes into various degrees of freedom such as ionization energy, thermal energy, ion internal excitation energy etc. Conversion of the laser light into X-rays depends on many parameters such as the atomic numbers of the target, the wavelength of the incident laser, the intensity of laser, the focal position etc. We have measured yield (conversion of laser energy to X-ray energy) of Ly_α, He_β, He_γ, He_δ, He_ε and Ly_β resonance lines which is found to be 0.54, 0.51, 0.41, 0.35, 0.29 and 0.13 μJ/sr respectively for incident laser energy 8.4 J.

3.5. Angular distribution:

Generally, X-ray emission from laser produced plasmas is assumed to be isotropic. However, several authors have reported an angular distribution of Bremsstrahlung X-ray flux in different X-ray spectral range using X-ray diodes covered with different filters [34]. In the majority of the measurements, the X-ray intensity is found to be some power law of cosθ, where θ is the angle between the detector and target normal. The spectral range in these measurements is very broad due to the X-ray filter which covers a large range of transmission. To use LPP X-ray sources for applications such as spectroscopy, materials studies and radigraphy, a narrow energy width (monochromatic) is required, which originates from line emission, especially resonance lines. It is important to know the angular distribution i.e intensity of resonance lines as a function of emission direction with respect to target normal. Plasma non-uniformity, opacity and eclipsing of hot plasma by the target at low take off angles are two important possibilities. Here, we have measured the X-ray emission of various radiative transition lines with respect to different angles.We have observed a large deviation from the isotropic nature of He- like resonance lines. The angular distribution of lines emitted from the K-shell have been studied by keeping the laser energy fixed

at 10 J.The angle between the crystal spectrometer and laser axis on target was changed by rotating the target with the help of a θ-stage. Each shot was taken on a fresh spot by moving it on a Y and Z stage. The angular distribution of various resonance lines He_β, He_γ, He_δ and He_ε are shown in Figure 6 a-d. From the figure, it is clear that the He_β line ($1s^2$-1s3p) has a higher level of anisotropy than lines with n=6 (i.e.$1s^2$-1s6p) which are less affected by plasma opacity. Lines corresponding to transitions from higher values of n are more appropriate for the calculation of plasma parameters. This justifies our decision to choose He_β and Ly_β for plasma parameter calculations. The TPS records of an Al plasma at various angle with respect to target normal at the same laser energy as used for X-ray measurements are shown in figure 6 e-g. It is clear from the figures that the flux of Al XII, Al XIII, Al XIV ions is decreasing when target normal is away from TPS. The results from the TPS support our measurement of angular dependency of X-ray intensities from various resonance lines.

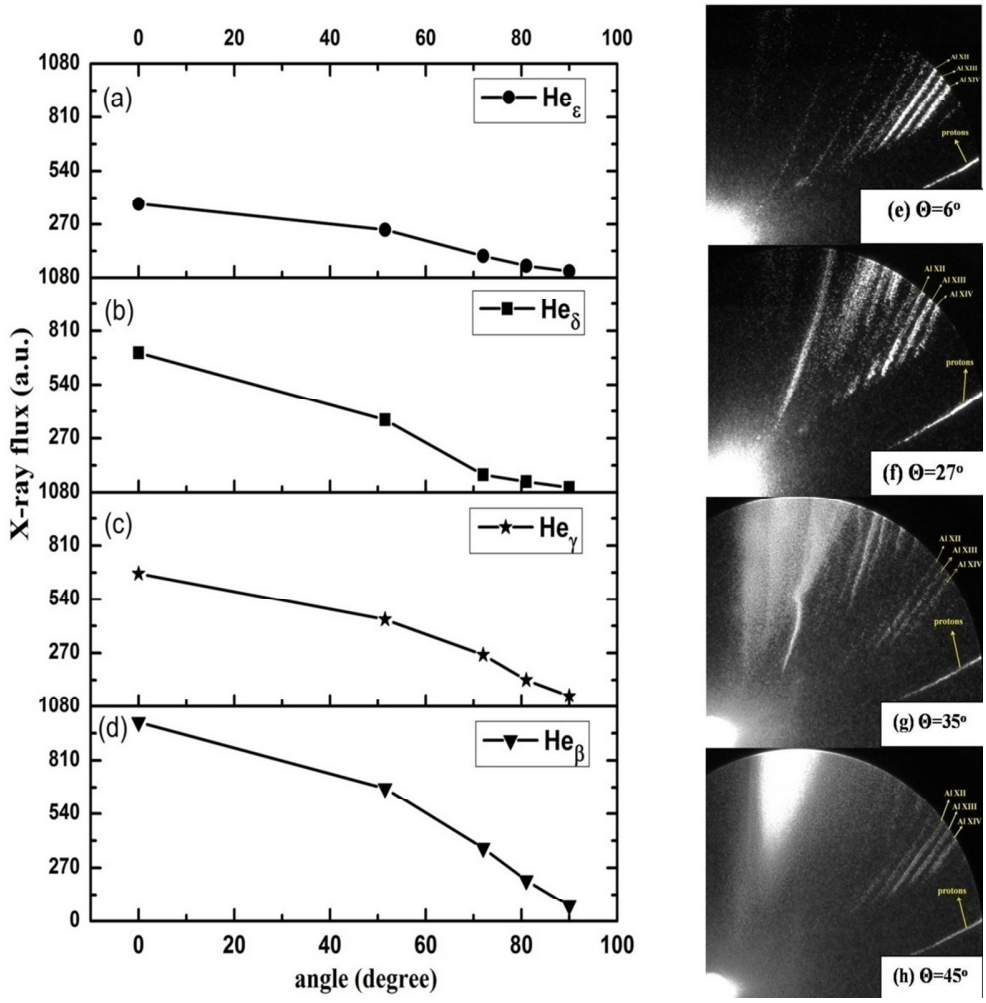

Figure 6.(a-d) Variation of intensity of K-shell resonance lines He$_\beta$, He$_\gamma$, He$_\delta$ and He$_\varepsilon$ with respect to different angles, **(e-h)** images of charge states of Al ions detected by Thomson parabola ion spectrometer at different angles between target normal and Thomson parabola ion spectrometer.

4.Conclusion:

K-shell X-ray emission spectra of Al plasma using a 30 J/500 ps Nd: glass laser with intensity 10^{13}-2x10^{14} W/cm^2 was studied. A scaling law of He-like resonance lines of Al plasma has been obtained and found to follow a power law $E \alpha I^{\alpha}$ with α=2.2, 2.3, 2.4 for He$_\beta$, He$_\gamma$, He$_\delta$ respectively. Plasma parameters have been derived by analyzing the K-shell emission spectra.The plasma temperature is calculated via the ratio

of Li-like satellites to the He_β line and the He-like satellite to the Ly_α line. The temperature and densities calculated by analytical models are 260 eV-420 eV and 1.6-2.8x10^{20} cm^{-3} respectively which is in good agreement with the results obtained by FLYCHK (T_e=160 eV, T_h=1 keV, f=0.008 and n_e=5x10^{20} cm^{-3}). The angular distribution of X-ray intensities has been found to vary significantly for low n lines e.g. He_β ($1s^2$-1s3p) where opacity effects reduce for higher values of transition states n i.e. He_γ, He_δ and He_ε. The angular variation in the ion number demonstates asimilar trend as the line emission.

Acknowledgement: The authors are grateful to Mr C G Murali for his help in smooth operation of laser system and Mr Ritesh Sable for his support in electronics being usd in laser power supplies and plasma diagnostics.

References:

[1] Loupias B, Perez F, BenuzziMounaix, Ozaki N, Rabec M, Gloahec LE. Highly efficient, easily spectrally tunable X-ray backlighting for the study of extreme matter states.Laser and Particles beams 2009; 27:601-609.

[2] Rossall AK, Gartside LMR, Chaurasia S, Tripathi S, Munda DS, Gupta NK et al. X-ray back-lighter characterization for iron opacity measurements using laser-produced aluminium K-alpha emission. J Phys B At Mol Opt Phys 2010; 15: 155403.

[3] Rybicki GB and Lightman AP. Fundamentals of Radiative Transfer. In: Radiative Processes in Astrophysics. New York: John Wiley & Sons Inc; 1979, p. 39

[4] Ruirong Wang, Weimin Chen, Chusheng Mao, Jiaqin Dong, and Sizu Fu. Laser-produced plasma He-alpha source for pulse radiography. Chinese Optics Letters 2009; 7:156-158.

[5] Lewis CLS, Mcglinchey. Quasi-monocromatic, Projection radiography of dense laser driven spherical targets.OptComm 1984; 53:179-186.

[6] Chaker M, Pépin H, Bareau V, Lafontaine B, Toubhans I, Fabbro R, et al. Laser plasma x-ray surces for microlithography. J Appl Phys 1988; 63:892-899.

[7] Förstera1 E, Gäbela K and Uschmanna I. X-ray microscopy of laser-produced plasmas with the use of bent crystals. Laser and Particle Beams 1989; 9:135-148.

[8] O'Neill F, TurcuICE, Tallents GJ, Dickerson J, Lindsay T, Goodhead DT , et al.A Repetitive Laser-Plasma X-Ray Source For Radiobiology Research. Proc. SPIE 1140, X-Ray Instrumentation in Medicine and Biology, Plasma Physics, Astrophysics, and Synchrotron Radiation 1989, 232.

[9] Lindl J. Development of the indirect-drive approach to inertial confinement fusion and the targets physics basis for ignition and gain. Physics of Plasmas1995; 2:3933-4024.

[10] Presnyakov LP. X-ray spectroscopy of high-temperature plasma. UspFizNauk 1976; 119:49-73.

[11] Biedermann C and Radtke R. Spectroscopy of heliumlike argon resonance and satellite lines for plasma temperature diagnostics. Phys Rev E: Stat Phys, Plasmas, Fluids 2002; 66:066404-9.

[12] Porquet D, Dubau J, Grosso N. He-like ions as practical astrophysical plasma diagnostics:From stellar coronae to active galactic nuclei. Space Science Reviews 2010; 157:103-134.

[13] Presnyakov LP and Urnov AM. X-ray plasma diagnostics. Journal de Physique 1979; 40:C7-279-C7-288.

[14] Boiko VA, FaenovAYa and PikuzSA . X-ray spectroscopy of multiply-charged ions from laser plasmas. J Quant SpectroscRadiatTransfer 1978; 19:11-50.

[15] Safronova UI, Safronova MS, Bruch R and Vainshtein LA.Dielectronic Satellite Spectra of the 1s3p-$1s^2$ lines for Highly-Charged Ions with Z=6-54. PhysicaScripta 1995; 51:471-483.

[16] Khatri I, Goyal A, Aggarwal S, Singh AK, Man Mohan. MCDHF calculations and study of plasma parameters for Li-like ions. Radiation Phys and Chem J 2016; 123:46-54

[17] Goyal A, Singh N, Aggarwal S, Singh AK and Man Mohan, Atomic structure calculation and study of line intensity ratio for Kr XXIV. Can J Phys ; DOI: 10.1139/cjp-2016-0167

[18] Gupta NK, Kumar V. Angular dependence of M and N band radiation and the effect of angular anisotropy on the total conversion efficiency of X rays emitted from a laser irradiated gold foil. Laser and Particle Beams 1995; 13:389-402.

[19] Vora HS, Nakhe SV, Sarangpani KK, Saxena P, Shirke ND and Bhatnagar R. Promise a software package for profile measurement of image size and edge enhancement.Centrefor Advanced Technology Report, CAT/95-10.

[20] Chaurasia S, Tripathi S, Leshma P, Murali CG, Pasley J. Optimization of bremsstrahlung and characteristic line emissionfrom aluminum plasma. OptComm 2013; 308:169-174.

[21] Yang J, Hu Zhimin, Zhang Jiyan, Zhu Tuo, Zhao Yang, Wen Tianshu, et al. High intensity x-ray line emission from aluminum plasmas generated by a 120 TW , 30fs laser pulse. Physics of Plasmas 2008; 15:112704-5.

[22] Gupta PD, Popil R, Fedosejevs R, Offenberger AA, Slazmann D and Capjack CE. Temperature and x-ray intensity scaling in KrF laser plasma interaction. Appl Phys Lett 1986; 48:103-6.

[23] Arora Vipul. X-ray Spectroscopic Studies of Plasma Produced by Intense Laser beams. Phd thesis

[24] Boiko VA, Pikuz SA,Safronova UI, FaenovAYa. Satellites to the He-like ion $1s^{21}S_o$- 1s3p $^1P_1$ lines with Z=12-19 in laser plasmas. Mon Not R AstronSoc 1978; 185:789-805.

[25] Gabriel AH and Paget TM. Measurement and interpretation of dielectronic recombination satellite line intensities. J Phys B: At Mol Opt Phys 1972; 5:673-685.

[26] Bely- Dabau F, Gabriel AH, Volonte S. Dielectronic satellite spectra for highly charges helium-like ions-III. Calculations of n=3 solar flare iron lines. Mon Not R AstronSoc 1979; 186:405-419.

[27] KonjevićN, Ivkovic M, Sakan N. Hydrogen Balmer lines for lowelectron number density plasma diagnostics. SpectrochimActa B2012;76:16–26.

[28] KonjevićN, Roberts JR. A critical review of the Stark widths andshifts of spectral lines from non-hydrogenic atoms.J Phys Chem RefData 1976;5:209–57.

[29] Olivero JJ, Longbothum RL. Empirical fits to the voigt line width: A Brief Review. Journal of Quantitative Spectroscopy and Radiative Transfer 1977;17:233–236.

[30] Vinodgradov AV,Sobel'man II,andYukov EA. Spectroscopic methods for diagnostics of superdense hot plasma. Sov J Quantum Electron 1974**;** 4**:**149-154.

[31] IIyukhin AA, Kramida AE, Peregudov GV, Chirkov VA. Determination of plasma electron densities from the intensity ratio of resonance and intercombination lines of helium-like ions. Sov J Quantum Electron 1981; 11:34-37.

[32] Naik PA, Nandwana PD, Gupta PD and Kumbhare SR. X-ray Spectroscopy in high temperature plasmas. B.A.R.C./I-911 (1987).

[33] Chung HK, Chen MH, Morgan WL, Ralchenko Y, and Lee RW.FLYCHK: Generalized population kinetics and spectral model for rapid spectroscopic analysis for all elements. High Energy Density Physics 2005;1:3-12.

[34] Kondo H, Tomie T. Optimisation of a laser-plasma x-ray source for contact microscopy. J Appl Phys 1994; 75:3798-3805.